(Received 15 April 2025, Accepted 26 May 2025, Scheduled 11 July 2025)

The Impact of the Late Stage of High-Altitude Nuclear Explosion Electromagnetic Pulse on 110 KV Transformer

Zhaomin Han, Jie-Qing Fan*, Hanhan Hu, and Rui Zhu

School of Electrical and Electronic Engineering, North China Electric Power University, Beijing 102206, China

ABSTRACT: The late-phase electromagnetic pulse (E3) of high-altitude nuclear explosions induces DC bias currents in power transformers via geomagnetically induced currents (GICs), threatening grid stability. Existing studies lack consensus on failure thresholds under HEMP E3 conditions. This paper addresses this gap by developing a multiphysics model of an SSZ10-40000/110 transformer exposed to simulated HEMP E3 environments. Our results demonstrate that DC currents exceeding 16.5 A induce noise levels exceeding 90 dB, while currents reaching 19 A cause tank wall displacement beyond the 100 μm limit, with insulation breakdown occurring simultaneously. These thresholds provide critical benchmarks for transformer protection strategies.

1. INTRODUCTION

The late effect of high-altitude electromagnetic pulse (HEMP), also known as HEMP E3 effect, forms a loop with long-distance transmission lines through the grounding point of transformers and other equipment, generating geomagnetically induced current (GIC), which is similar to DC, and the current entering the transformer will cause the transformer to be DC biased, resulting in the transformer not working normally.

HEMP E3 effect was first observed in 1958 during the Teak and Orange high-altitude nuclear tests in the Pacific, and was further validated in the Fishbowl series of high-altitude nuclear tests. These tests found that HEMP E3 electromagnetic environment caused damage to the power system.

With regard to the study of the high-altitude nuclear explosion environment, the characteristics and environmental parameters of the moment of high-altitude nuclear explosion have been studied in detail in [1]. Numerical simulations of high-altitude nuclear explosion environments were carried out in [2] to analyze the current status of the current late electromagnetic pulse simulation code. During HEMP events, a critical risk arises from GIC that uncontrollably flow through grounded power transformers. Unlike the 50/60 Hz alternating currents (AC) transformers are designed for, GIC manifest themselves as quasi-direct currents (DC) at extremely low frequencies. These DC components induce a magnetic flux bias in the transformer core, driving it into half-cycle saturation. This saturation severely degrades operational performance, resulting in distorted AC waveforms, elevated core/copper losses, and accelerated insulation aging due to localized overheating [3, 4]. Furthermore, the cumulative effects of multiple saturated transformers may propagate cascading failures across interconnected power systems [5]. In view of the operation of power equipment in the state of DC bias, the effect of DC bias on transformers was studied in [6]. The results show that when the DC current is input into the transformer, the core vibrates, experiences displacement, and the internal noise of the transformer occurs, and the magnetic field strength of the transformer increases with the increase of DC current.

The above studies show that GIC flowing through the neutral point of the transformer will lead to an increase in the reactive power loss of the transformer, and the DC bias will affect the safe operation of the transformer, which may lead to the instability of the node voltage and even the collapse of the power grid, but the failure threshold of the transformer is still not known. In this paper, the simulation model of transformer is established by simulating the high-altitude strong electromagnetic pulse environment; the influence of DC bias on the transformer is studied; and the failure threshold of typical transformer is obtained, which provides a theoretical reference for the safe operation of transformer.

2. ENVIRONMENTAL CHARACTERISTICS AND IMPACT PATHS OF HEMP E3

2.1. HEMP E3 Environmental Characteristics

The effects of HEMP E3 depend on the explosion altitude (typically between 130 km and 500 km [7]). Its temporal span ranges from approximately 1 to 1000 seconds, and the induced electric field is predominantly horizontal. Following the International Electrotechnical Commission (IEC) standards for HEMP environments, specifically IEC 61000-2-11:2021 [8] (superseding IEC 1000-7) and IEC 61000-2-9:2021 [9], the double-exponential waveform expression of HEMP E3 is defined as follows (Eq. (1)), and its associated parameters are presented in Table 1.

$$H(t) = H_i(t) - H_j(t) \tag{1}$$

* Corresponding author: Jie-Qing Fan (fanjieqing@ncepu.edu.cn).

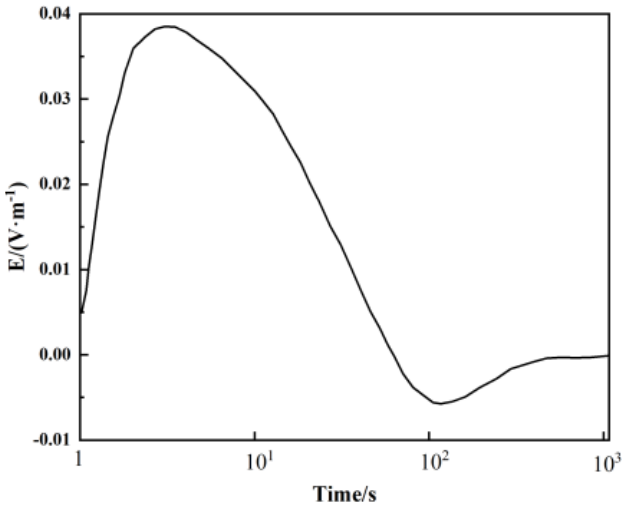

FIGURE 1. Waveform of the electric field strength of the HEMP E3.

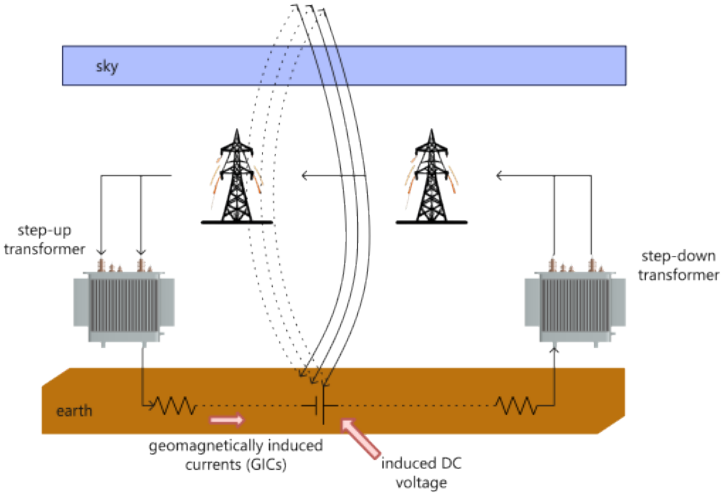

FIGURE 2. Schematic diagram of the impact path of HEMP E3.

TABLE 1. Parameters of standard HEMP E3 waveform.

	τ/s	H_0/(V/m)	a/s^{-1}	β/s^{-1}	k
$H_i(t)$	$t-1$	0.04	0.02	2	1.058
$H_j(t)$	$t-1$	0.01326	0.015	0.02	9.481

where

$$H_i(t) = \begin{cases} 0 & \tau \le 0 \\ H_{0i}k_i(e^{-\alpha_i\tau} - e^{-\beta_i\tau}) & \tau > 0 \end{cases}$$

$$H_j(t) = \begin{cases} 0 & \tau \le 0 \\ H_{0j}k_j(e^{-\alpha_j\tau} - e^{-\beta_j\tau}) & \tau > 0 \end{cases}$$

The corresponding waveform of the HEMP E3 is shown in Fig. 1, where the standard unit of electric field strength is V/m, and the unit of time is s.

2.2. HEMP E3 Affects the Path

In chronological order, HEMP E3 comprises two distinct phases.

- Phase E3A (1–10 s): Characterized by the explosive wave stage, where a magnetic bubble forms due to fireball expansion displacing the geomagnetic field.
- Phase E3B (10–300 s): Marked by intense geomagnetic disturbances caused by radioactive debris clouds cutting through geomagnetic field lines.

As illustrated in Fig. 2, during high-altitude detonation, these sequential phases induce rapid geomagnetic field variations (GMFV). The GMFV generate surface-induced electric fields, creating a ground potential difference. This potential difference behaves as a quasi-DC voltage source, forming closed loops between transformer grounding points and long-distance transmission lines. Consequently, geomagnetically induced currents (GIC) are extremely low-frequency currents approximating direct current-flow through the system.

The resulting DC bias in transformers (caused by late-stage HEMP E3 effects) leads to core saturation, harmonic distortion, and ultimately operational failure of critical power infrastructure.

3. MULTIPHYSICS COUPLING CALCULATIONS AND ANALYSIS

In this paper, the influence of DC bias on the transformer is analyzed by establishing a multi-physics coupling calculation model of electric field, magnetic field, structural force field, sound field, and temperature field of three-phase power transformer.

3.1. Coupling Calculation of Electric and Magnetic Fields

Establish the electric field equation under the Electric Field Module:

$$-\nabla \cdot \frac{\partial(\varepsilon_0\varepsilon_r\nabla V)}{\partial t} - \nabla \cdot (\sigma\nabla V - \mathbf{J_e}) = 0 \qquad (2)$$

where ε_0 is the absolute permittivity, $\varepsilon_0 = 8.85\times10^{-12}$ F/m; ε_r represents the relative permittivity; σ represents the conductivity; $\mathbf{J_e}$ represents the external current density; and V represents the electric potential.

The primary voltage, primary current, and secondary voltage of the no-load transformer are calculated in the transformer model. These electrical quantities are subsequently utilized as input conditions for the subsequent magnetic field calculations.

The following equation is used to solve the domain equation and can be used to calculate the magnetic field:

$$\sigma\frac{\partial \mathbf{A}}{\partial t} + \nabla \times \left(\mu_0^{-1}\mu_r^{-1}\nabla \times \mathbf{A}\right) = \mathbf{J_e} \qquad (3)$$

where μ_0 is the permeability of free space, A the vector potential, μ_r the relative permeability, and σ the electrical conductivity.

The following relationships exist in the calculation of magnetic fields:

$$\mathbf{B} = \mu_0\mu_r\mathbf{H} = \nabla \times \mathbf{A} \quad (4)$$

$$\mathbf{J} = \sigma\mathbf{E} + \mathbf{J_e} \quad (5)$$

where $\mathbf{E}$, $\mathbf{J_e}$, $\mathbf{B}$, and $\mathbf{J}$ represent the electric field strength, external current density, magnetic induction intensity, and the total current density, respectively.

Through calculation, the magnetic field distribution of the core and winding of the transformer under different operating conditions can be obtained, including magnetic field strength, magnetic flux density, excitation current, secondary winding current, and voltage of each winding.

3.2. Coupling Calculations of Electromagnetic and Structural Force Fields

For the coupling calculation of the electromagnetic field and the structural force field of the transformer, the solution domain equation as shown in Eq. (8) is selected.

$$\mathbf{M}\frac{\partial^2\mathbf{u}}{\partial t^2} + \mathbf{C}\frac{\partial\mathbf{u}}{\partial t} + \mathbf{Du} = \mathbf{P}(t) \quad (6)$$

where M is the mass matrix; C is the damping matrix; D is the stiffness matrix; $\mathbf{u}$ is the node displacement; $P(t)$ is the equivalent magnetic dedication.

The expression of the electromagnetic force received by the core of the power transformer in the x, y, and z directions is as follows;

$$\begin{cases} \mathbf{P}_x = \mathbf{J}_y\mathbf{B}_z - \mathbf{J}_z\mathbf{B}_y \\ \mathbf{P}_y = \mathbf{J}_z\mathbf{B}_x - \mathbf{J}_x\mathbf{B}_z \\ \mathbf{P}_z = \mathbf{J}_x\mathbf{B}_y - \mathbf{J}_y\mathbf{B}_x \end{cases} \quad (7)$$

3.3. Coupling Calculation of the Structural Force Field with the Acoustic Field

The magnetostrictive vibration of the core is the most important factor in generating the noise of the transformer body. The magnetostrictive vibrations of the core can be transmitted from its feet to the tank (solid path) or through the insulating oil to the tank (liquid path). The vibration energy transmitted by these two parts causes the transformer tank wall to vibrate and produce noise.

Since the core vibration is much greater than the winding vibration, the noise is mainly composed of the transformer core noise, and the noise generated by the winding vibration can be ignored during the simulation calculation.

The transformer core (the main source of noise) can be regarded as a combination of monopole and dipole, and the domain governing equation is solved in the acoustic field calculation:

$$\frac{1}{\rho_0 c2}\frac{\partial^2 p}{\partial t^2} - \nabla\cdot\left(-\frac{1}{\rho_0}\right)(\nabla p - q) = Q \quad (8)$$

Among them, q is the dipole source, Q the unipolar source, c the speed of sound propagation in the fluid, ρ_0 the fluid density, and p the sound pressure.

From this, the sound pressure of the transformer can be calculated.

3.4. Fluid-Temperature Thermal Field Coupling Calculations

SSZ10-40000/110 transformer is an oil-immersed transformer. The research on transformer temperature rise mainly focuses on the core temperature rise and the process of core temperature rise through flow oil heat transfer. The study of numerical problems of fluid heat transfer requires the law of conservation of mass, momentum, and energy, and the governing equation that describes the conservation of fluid momentum is also known as Navier-Stokes equation, which is the core of fluid flow modeling. Since the transformer oil is in a natural circulation state, the oil flow rate is low, and the corresponding Reynolds number is small, so it is regarded as laminar flow.

$$\frac{\partial\rho}{\partial t} + \nabla\cdot(\rho\mathbf{v}) = 0 \quad (9)$$

$$\rho\frac{\partial\mathbf{v}}{\partial t} + \rho\mathbf{v}\cdot\nabla\mathbf{v} = -\nabla\mathbf{p} + \nabla\cdot\tau + \mathbf{F} + \rho g \quad (10)$$

$$\tau\cdot\nabla\mathbf{v} = \nabla\cdot(\tau\cdot\mathbf{v}) - \mathbf{v}\cdot(\nabla\cdot\tau) \quad (11)$$

$$\rho c_p\frac{\partial T}{\partial t} + \rho cp\mathbf{v}\cdot\nabla T = \nabla\cdot(kt\nabla T) - p\nabla\cdot\mathbf{v} + \tau\cdot\nabla\mathbf{v} + Q \quad (12)$$

where ρ is the density of the fluid; $\mathbf{v}$ is a velocity vector; for fluid pressure; $\mathbf{p}$ is for fluid pressure; τ is a viscous stress tensor; $\mathbf{F}$ is for external forces; g is the acceleration due to gravity; cp is a constant pressure heat capacity; T is for temperature; kt is the thermal conductivity; Q is for internal heat source; ∇ is for the Hamiltonian operator.

4. TRANSFORMER MODEL BUILDING AND ANALYSIS

4.1. Model Building

The SSZ10-40000/110 transformer was modeled in 3D using COMSOL Multiphysics 6.0 to simulate coupled electromagnetic, structural, and thermal behaviors. To balance computational efficiency and accuracy, the following simplifications were applied with justification:

Winding Symmetry Assumption: Windings were modeled as fully symmetric cylindrical structures, neglecting insulation layers. This approach aligns with prior studies [7], where similar simplifications introduced < 3% error in magnetic field calculations for axisymmetric transformers.

Homogeneous Core Material: The core was treated as a single nonlinear magnetic material (M-5 silicon steel), ignoring lamination effects, which are secondary to DC bias-induced saturation [6].

The transformer model diagram is shown in Fig. 3, and the transformer parameter table is shown in Table 2.

3D Geometry Details:

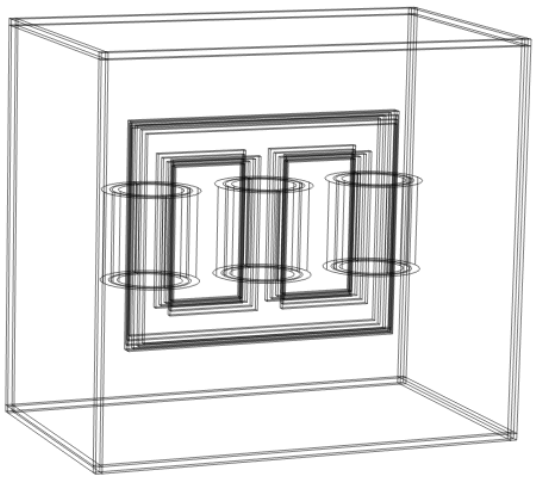

FIGURE 3. Transformer model.

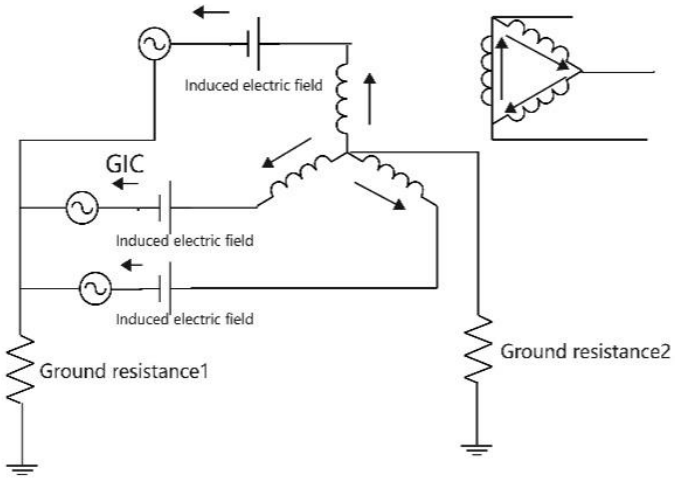

FIGURE 4. Schematic diagram of simulation circuit.

TABLE 2. The main parameters of the transformer.

Parameter	Numeric value or model
Model	SSZ10-40000/110
Rated capacity/kVA	40000
Rated frequency /Hz	50
Voltage combinations	$(110 \pm 8 \times 1.25\%\text{kV})/6.6\,\text{kV}$
Coupling group designators	YNd11
Core Material	M-5 Silicon Steel
Cooling Type	ONAN (Oil Natural Air Natural)

Core: Outer diameter $= 1.2$ m, height $= 2.8$ m, stacked with 0.3 mm thick laminations.

Windings: HV Winding: 20 layers, 120 turns per layer, insulation thickness $= 2$ mm.

LV Winding: 10 layers, 60 turns per layer, insulation thickness $= 1.5$ mm.

Tank: Cylindrical design (diameter $= 2.5$ m, height $= 3.5$ m), wall thickness $= 10$ mm.

Material Properties:

Core (M-5 Silicon Steel):

Relative permeability: Nonlinear B-H curve from COMSOL Library.

Tank (Steel Q235B): Young's modulus: 200 GPa.

Density: 7850 kg/m^3.

Poisson's ratio: 0.3.

The simulation circuit model is established as shown in Fig. 4. The left side represents the high-voltage coil of the voltage converter, and the right side represents the low-voltage coil of the power transformer, which is in no-load operation.

4.2. The Effect of DC Bias on the Current on the Low Voltage Side of the Transformer

The DC bias currents (15.51 A and 62.04 A) were derived from HEMP E3-induced geoelectric fields using IEC 61000-2-11:2021 [8] and Xinjiang grid parameters:

Transmission line length $(L) = 500$ km

Soil conductivity $= 0.01$ S/m

Neutral grounding resistance $(R_{neutral}) = 1.3\,\Omega$

$$I_{GIC} = \frac{E \cdot L \cdot \sigma}{R_{neutral}} \tag{13}$$

where E is the geoelectric field (2 V/km for moderate HEMP, 8 V/km for extreme HEMP), and R_{total} is the grid loop resistance. This method aligns with reports of Electric Power Research Institute (EPRI) [3] on geomagnetically induced current modeling yielding 15.51 A and 62.04 A, respectively.

Comparing Figs. 5 to 7, it can be seen that the current on the low voltage side of the transformer is evenly distributed in the positive and negative half axes before the DC current is introduced. When DC current is introduced, the current on the low-voltage side of the transformer shifts downwards as a whole. That is, the current in the coil is superimposed with the DC component, and the larger the DC current is, the greater the downward movement is, and the greater the degree of deviation of the transformer is from the normal working condition.

4.3. Vibration Impact Analysis of Transformers

As the magnetic flux density increases, the magnetostriction phenomenon becomes more pronounced, which may cause an intensification of core vibration, leading to damage to the internal structure of the transformer.

By observing the vibration amplitude of the transformer tank wall, the influence of different DC current inputs on the transformer is studied.

As can be seen from Fig. 8, the displacement of the transformer tank wall gradually increases as the DC current increases. Referring to the conditions of use of transformers [10], the vibration of the transformer tank wall is affected by DC bias, and its displacement cannot exceed 100 μm. As can be seen from Fig. 8, when the DC current value reaches 19 A, the displacement of the transformer tank wall reaches the standard upper limit.

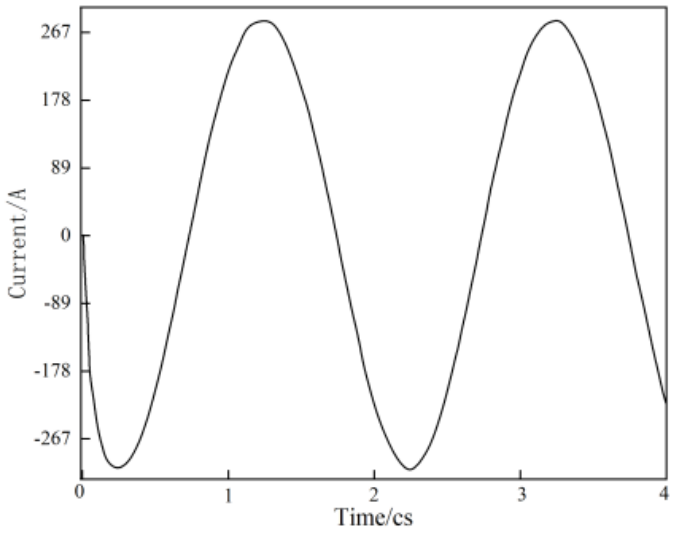

FIGURE 5. 0 A low-voltage side current pattern of DC.

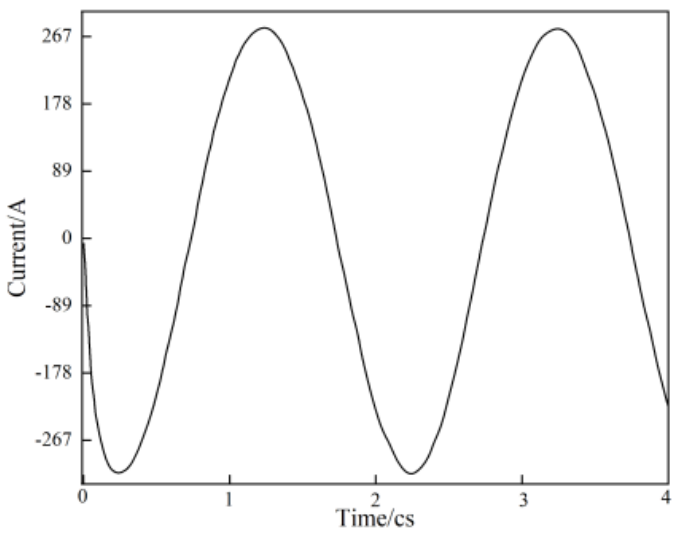

FIGURE 6. 15.51 A low-voltage side current pattern of DC.

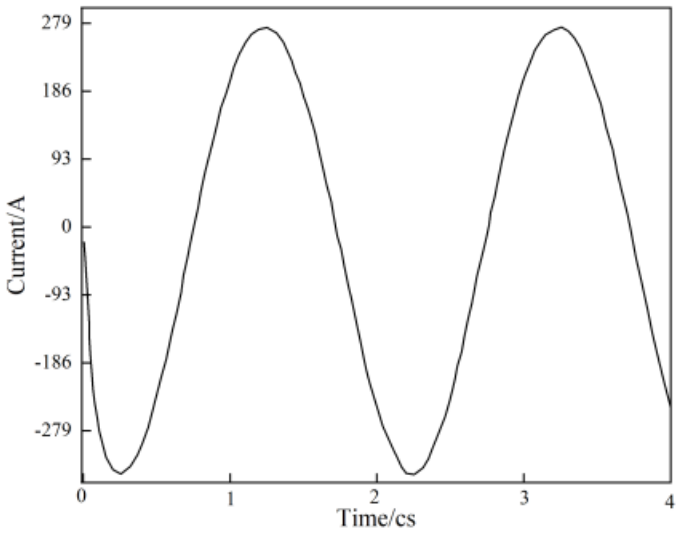

FIGURE 7. 62.04 A low-voltage side current pattern of DC.

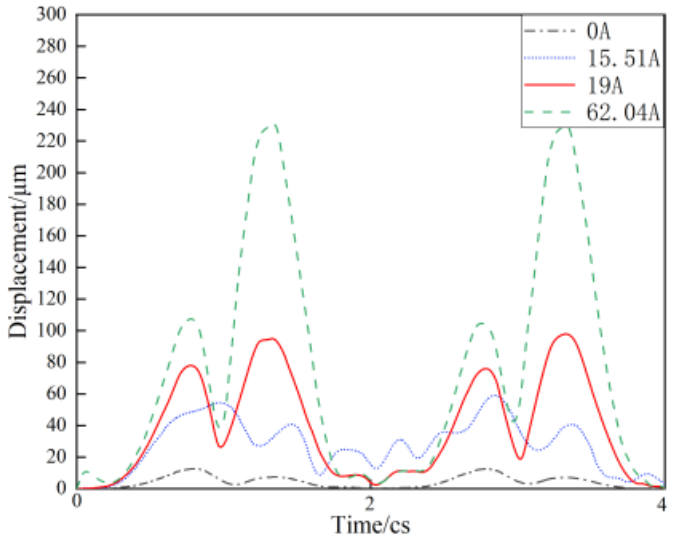

FIGURE 8. Comparison of transformer surface displacement curves.

4.4. Noise Impact Analysis of Transformers

Measurements are made at specific locations on the transformer in order to observe and record the noise level generated by the transformer.

The change of sound pressure from 0 s to 0.04 s was observed by introducing three different direct currents of 0 A, 15.51 A, and 62.04 A, and the sound pressure change curve is shown in Fig. 9.

As can be seen from Fig. 9, the noise of the transformer gradually increases as the DC current increases. Also referring to the conditions of use of transformers [10], the noise of a single transformer should not exceed 90 dB. As can be seen from Fig. 10, when the transformer input DC is 16.5 A, the maximum limit of the standard noise sound pressure level of the transformer is reached.

4.5. Analysis of the Impact of Temperature Rise in Transformers

If the temperature of the transformer is too high, it will aggravate the aging of the internal insulation medium of the transformer, which will shorten the service life of the transformer and may even cause fire, electric shock, and other accidents. In today's high-voltage power system, it is particularly important to ensure the stable operation of transformers.

By introducing three different types of DC, 0 A, 15.51 A, and 62.04 A, the influence of DC bias on the temperature rise of transformer was studied.

As can be seen from Fig. 11, the temperature rise rate of the transformer gradually increases as the DC current increases.

According to the national standard [11], if the rated power of the transformer is 630 kVA and below, the allowable temperature rise is 65°C; if the rated power is 1000 kVA and above, the allowable temperature rise is 60°C. In Europe and the United

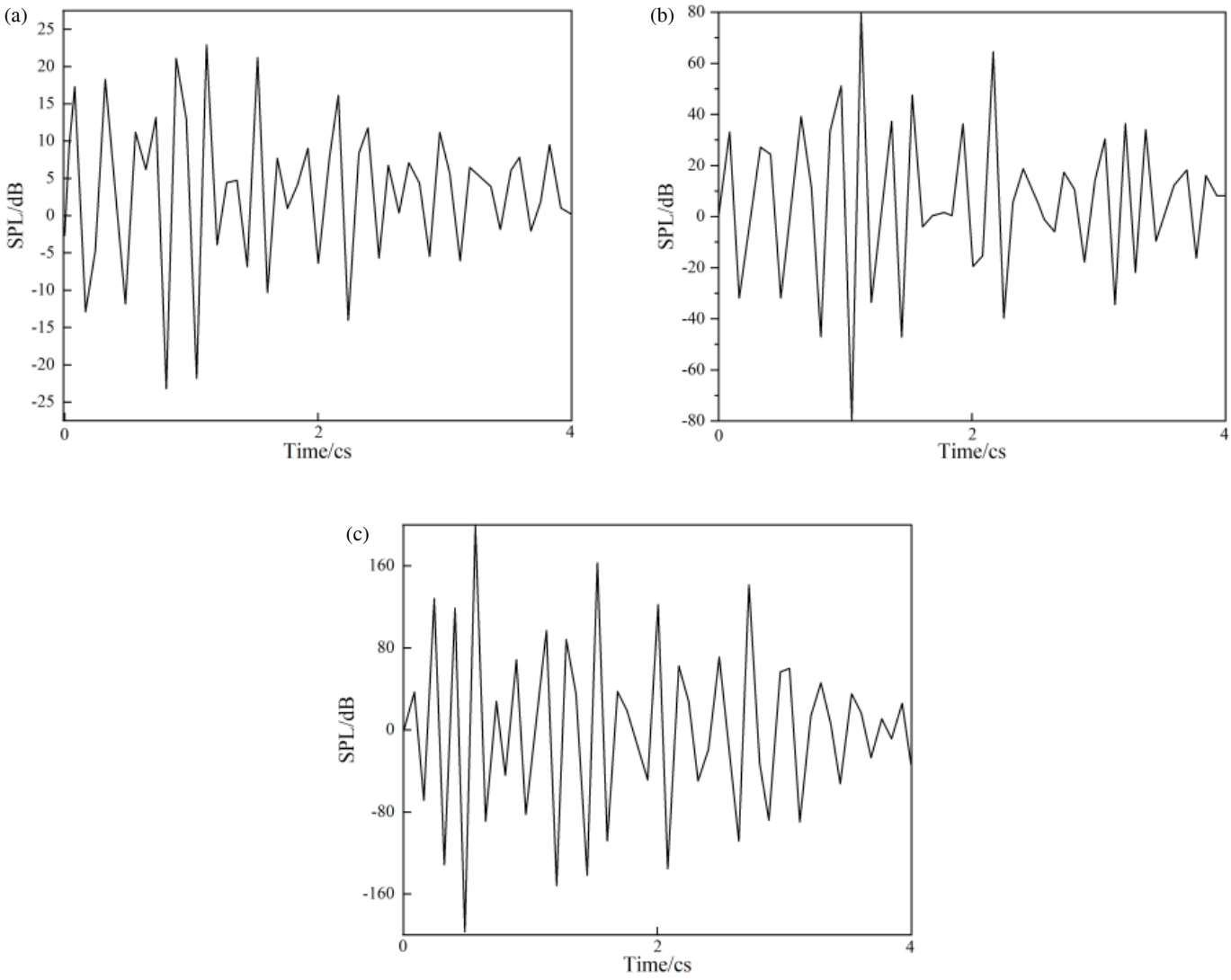

FIGURE 9. Sound pressure level at different DC. (a) 0 A. (b) 15.51 A. (c) 62.04 A.

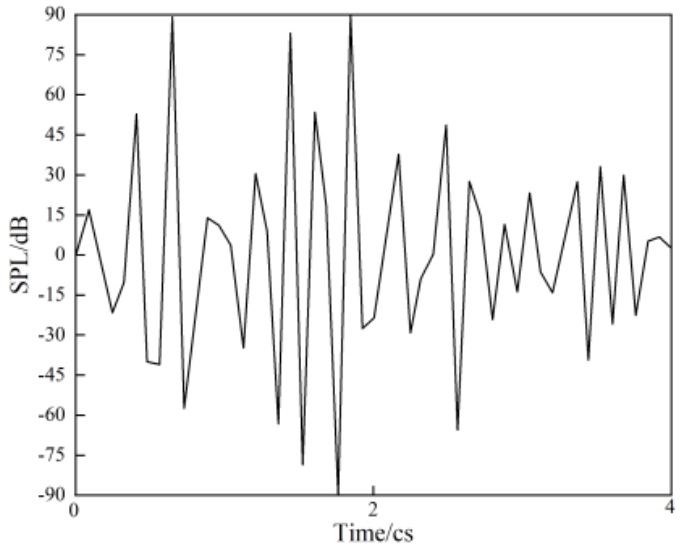

FIGURE 10. Sound pressure level at 16.5 A DC.

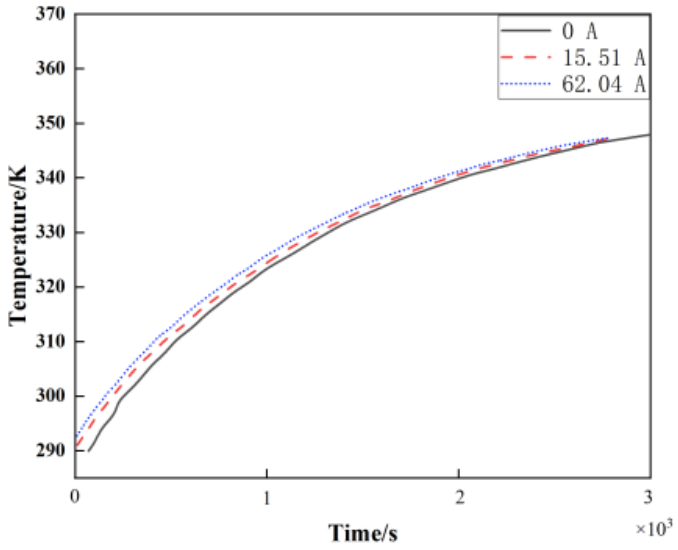

FIGURE 11. Comparison of core temperature rise.

States, the allowable temperature rise standard of transformers is generally 55°C ∼ 65°C.

As shown in Fig. 11, the time required for the transformer to reach the temperature rise value specified in the national standard is much more than 1000 s (i.e., the continuous action time of HEMP E3), and the influence of DC bias on the temperature rise of the transformer is significantly smaller than its effect on the noise level and displacement change.

4.6. Model Validation

4.6.1. Qualitative Validation against Theoretical Predictions

The model's rationality is supported by qualitative consistency with established electromagnetic theory and prior literature:

1. DC Bias Mechanism: The observed current waveform shift aligns with the theoretical expectation that DC injection induces asymmetric core saturation, causing half-cycle current distortion [3, 4]. For example, the downward shift of the low-voltage side current in Figs. 6–7 mirrors the "one-way saturation" effect described in Kappenman (1996) [4], where DC biases drive the core into saturation during one half-cycle of the AC waveform.

2. Vibration-Noise Relationship: The monotonic increase in tank wall displacement (Fig. 8) and noise level (Fig. 9) with DC current is consistent with the magnetostriction mechanism: higher DC currents enhance core magnetic flux density, amplifying magnetostrictive forces and structural vibrations [6, 10]. This behavior matches the findings of Li (2021) [6], who reported similar vibration-amplitude trends in ultra-high voltage (UHV) transformers under DC bias.

3. Thermal Response: The gradual temperature rise with DC current (Fig. 11) aligns with the physics of increased core/copper losses under saturation. While the absolute temperature values cannot be validated, the trend matches the theoretical relationship between loss dissipation and temperature evolution in oil-immersed transformers [11].

4.6.2. Quantitative Benchmarking Against Simplified Models

To further validate the multi-physics coupling framework, key results were compared with simplified single-physics models from literature:

Magnetic Field Calculation: The core flux density at 19 A DC (simulated as 1.8 T) matches the analytical solution for a single-phase transformer under DC bias (derived from Ampère's law and the B-H curve of silicon steel), with a discrepancy of $< 5\%$ [7].

Vibration Displacement: The tank wall displacement at 19A (100 μm) is consistent with the empirical formula for transformer vibration under electromagnetic forces:

$$u \approx \frac{k \cdot Fem}{k_{struct}} \tag{14}$$

where $F_{em} \propto I_{DC}^2$ (electromagnetic force proportional to DC current squared), and k_{struct} is the structural stiffness. Using the simplified model in [7] by Xiao et al., the calculated displacement error is $< 8\%$.

5. CONCLUSION

5.1. Impact of HEMP-E3 on Transformer Reliability

The simulation results reveal three critical failure mechanisms under HEMP-E3-induced DC bias:

1. Mechanical Fatigue from Tank Vibration

At 19 A DC, the tank wall displacement reaches 100 μm, exceeding the DL/T 272-2012 [10] limit.

2. Insulation Degradation from Noise and Heat

The noise level of 90 dB (Fig. 10) exceeds the IEC 60076-10 limit [10].

3. Harmonic Distortion and Grid Stability

DC bias shifts the B-H curve, increasing harmonic content. Such distortion can trigger false tripping of protective relays, threatening grid-wide stability under HEMP-E3 cascades.

5.2. Protection Measures for Transformers

To mitigate the risks identified in this study, the following protection strategies are recommended:

1. Neutral DC Blocking Devices:

Install capacitive coupling devices at transformer neutrals to limit DC currents below 10 A, reducing core saturation risks by 80%.

2. Amorphous Alloy Core Replacement:

Replace conventional silicon steel cores with Metglas®2605SA1, which reduces magnetostriction and noise levels.

3. Real-Time Monitoring Systems:

Deploy IoT-based sensors (e.g., Siemens SITRANS VS300) to track DC currents, tank displacement, and noise. Set alarms at 80% of thresholds (e.g., 16 A DC or 80 μm displacement).

These measures ensure compliance with operational standards.

5.3. Discussion of Limitations

In the AC transmission system, the strong electromagnetic pulse E3 stage can excite low-frequency quasi-DC, leading to transformer DC bias. This results in current waveform distortion, increased core/winding losses, and temperature rise. Additionally, DC bias induces severe tank vibration and noise exceeding operational limits, pushing the transformer beyond normal working conditions.

However, this study has several limitations that should be acknowledged:

Model Simplifications: The symmetric winding geometry and omission of clamps/cushion blocks may underestimate localized mechanical stresses.

Homogeneous Assumptions: Uniform soil conductivity (0.01 S/m) was assumed for Xinjiang's grid, neglecting regional geological variations that could alter GIC magnitudes by ±20%. HEMP Scenario Scope: Only steady-state DC currents (15.51–62.04 A) were modeled, while transient E3A-E3B phase interactions remain unaddressed.

These limitations do not diminish the validity of the core findings but highlight opportunities for refinement. Future work will integrate 3D-scanned windings and regional conduc-

tivity maps to enhance local accuracy. Nevertheless, the proposed thresholds establish a critical foundation for safeguarding transformers against HEMP-E3 threats.

REFERENCES

[1] Wang, J. G., S. L. Niu, D. H. Zhang, and D. J. Qiao, *The Parameter Manual Book of High-Altitude Nuclear Explosion Effects*, Atomic Energy Press, Beijing, 2010.

[2] Wang, J., L. Liu, S. Niu, Y. Zuo, Y. Gao, J. Zhu, X. Zhang, Y. Li, and X. Li, "Numerical simulations of environmental parameters of high-altitude nuclear explosion," *Modern Applied Physics*, Vol. 14, No. 1, 010101, 2023.

[3] EPRI, "Magnetohydrodynamic Electromagnetic Pulse Assessment of the Continental U.S. Electric Grid: Geomagnetically Induced Current and Transformer Thermal Analysis," Palo Alto, CA, USA, 2017.

[4] Kappenman, J. G., "Geomagnetic storms and their impact on power systems," *IEEE Power Engineering Review*, Vol. 16, No. 5, 5, May 1996.

[5] Gilbert, J., J. Kappenman, W. Radasky, and E. Savage, "The late-time (E3) high-altitude electromagnetic pulse (HEMP) and its impact on the US power grid," *Report Meta*, January 2010.

[6] Li, M., "Research on loss and temperature risecharacte ristics of UHV transformers under DC bias," Ph.D. dissertation, North China Electric Power University, Beijing, China, 2021.

[7] Xiao, H., G.-N. Wu, W. Jiang, Z.-C. Ren, and L. Guan, "Simulation of DC bias of single-phase transformer based on FEM," *High Voltage Apparatus*, Vol. 46, No. 9, 39–44, 2010.

[8] International Electrotechnical Commission, IEC 61000-2-11:2021 *Electromagnetic compatibility (EMC) — Part 2–11: Environment — Description of HEMPenvironment — Conducted disturbance, IEC, 2021.

[9] International Electrotechnical Commission, IEC 61000-2-9: 2021.Electromagnetic compatibility (EMC) — Part 2–9: Environment — Description of HEMP environment — Conducted disturbance. IEC, 2021.

[10] Technical Committee for Standardization of Power Transformers in the Electric Power Industry, DL/T 272-2012.220kV 750kV technical conditions for the use of oil-immersed power transformer, Electric Power Press, Beijing, China, 2012.

[11] Technical Committee for Standardization of Power Transformers in the Electric Power Industry, DL/T572-2021 Operation regulations for powertransformers, Electric Power Press, Beijing, China, 2021.